Robust Optimization to Reduce Dose Delivery Uncertainty by Potential Applicator Displacements for a Cervix Brachytherapy

Byungdu Jo
Yonsei University - Wonju Campus https://orcid.org/0000-0001-7349-6631
Kyeongyun Park
National Cancer Center
Kwang Hyeon Kim
National Cancer Center
Dongho Shin
National Cancer Center
Young Kyung Lim
National Cancer Center
Jong Hwi Jeong
National Cancer Center
Se Byeong Lee
National Cancer Center
Hee-Joung Kim
Yonsei University - Wonju Campus
Haksoo Kim (haksoo.kim@ncc.re.kr)
https://orcid.org/0000-0001-8983-5423

Research

Keywords: Robust optimization, Genetic algorithm, Brachytherapy, Multi-objective, Median absolute deviation

Posted Date: February 4th, 2020

DOI: https://doi.org/10.21203/rs.2.22610/v1

Robust Optimization to Reduce Dose Delivery Uncertainty by Potential Applicator Displacements for a Cervix Brachytherapy

Byungdu Jo [1, 2], Kyeongyun Park[2], Kwang Hyeon Kim[2], Dongho Shin[2], Young Kyung Lim[2], Jong Hwi Jeong[2], Se Byeong Lee[2], Hee-Joung Kim[1*], Haksoo Kim[2*]

[1]Department of Radiological Science, College of Health Science, Yonsei University, Wonju, Korea.

[2]Proton Therapy Center, National Cancer Center, Goyang, Korea

* These authors are considered as co-corresponding authors

Correspondence to:

Hee-Joung Kim, email: hjk1@yonsei.ac.kr, phone: +82-33-760-2475

Haksoo Kim, email: haksoo.kim@ncc.re.kr, phone: +82-31-920-1757

Abstract:

Background:

Applicator displacement during brachytherapy treatment for cervical cancer leads to a drastic change in dose distribution. Hence, applicator displacement uncertainty is of significant relevance within the distribution of dose prescription. To minimize applicator displacement from patient movement during cervical cancer brachytherapy treatment, a multi-objective genetic algorithm was combined with a median absolute deviation (MAD) constrained

robust optimization concept.

Materials and methods:

To evaluate the feasibility of the robust optimization algorithm on applicator displacements, the clinically applied treatment plans of six tandem and ring (T&R) applicator cases for cervical cancer were included. All patients underwent magnetic resonance imaging (MRI) after the placement of the T&R applicator. The method considered multiple random scenarios reflecting the uncertainties in the dose delivered. For simplicity, the uncertainties in this proof-of-concept study were limited to potential applicator displacements. This problem is optimized by MAD-constrained robust optimization using a patient-specific multi-objective genetic algorithm. The proposed approach is then compared against the nominal (manual) plan strategies.

Results:

All generated plans fulfilled EMBRACE protocol guidelines for all targets and organs at risk (OAR). MAD-constrained robust optimization provided not only excellent target coverage but also minimized doses to OAR. The nominal and robust plan equivalent dose in 2 Gy fractions (EQD2) of D98 for high-risk clinical target volume (HR-CTV) and rectum were 88.59, 55.29, and 84.84, 54.09, respectively. Furthermore, each standard deviation of D98 for HR-CTV and rectum reduced from ±1.0177 to ±0.9085 and ±0.4927 to ±0.4052, respectively.

Conclusions:

Definitive dwell times and positions by the use of robust planned external beam radiation therapy plus brachytherapy (EBRT-BT) boost for cervical cancer were well tolerated. Using this robust strategy, the generated plans showed an increase in target coverage and minimized applicator displacement impact uncertainty on dose delivery.

Keywords: Robust optimization, Genetic algorithm, Brachytherapy, Multi-objective, Median absolute deviation

1. Background

Cervical cancer is the fourth most frequent cancer among women worldwide, with an annual incidence of 570,000 cases and 311,000 deaths in low- and middle-income countries in 2018. It ranked second for both incidence and mortality in the lower Human Development Index (HDI) among women [1, 2]. According to previous reports, cervical cancer patients with initial stages (stages IB – IIA) who undergo appropriate treatment will develop recurrence with a risk factor of 10 – 15% [3, 4]. Therefore, early diagnosis and treatment of cervical cancer are crucial for reducing the mortality rate.

One of the most common treatment strategies for cervical cancer, when high dose radiation is required to be curative, is a combination of external beam radiotherapy (EBRT), chemotherapy and brachytherapy, such as EBRT alone, EBRT plus brachytherapy, or combined EBRT plus brachytherapy with concurrent chemotherapy [5]. Several studies have verified that the combination of EBRT, chemotherapy, and brachytherapy improves treatment outcomes in cervical cancer [6-8]. It is well known that the brachytherapy boost improves outcomes due to its superiority of rapid dose fall-off with distance from the source and limited dose exposure of surrounding tissues in accordance with the inverse square law [9]. Moreover, a remote after-loading platform, including radioactive sources, allows for a more precise configuration of the dose to the target and the optimization of dwell times [10].

Excellent results are achieved with brachytherapy in combination with EBRT, although this approach is not free from limitations. The dose distribution in brachytherapy has a sharp dose gradient of which is inherent to the radioactive source, and it is more sensitive to patient setup and applicator position uncertainties [11]. Uncertainties in brachytherapy for cervical cancer are mainly related to source calibration, dose and dose-volume-histogram (DVH) calculation, reconstruction of applicators, contouring, intra- and inter-fraction uncertainties and dose delivery [12-19]. Moreover, in MRI/computed tomography (CT)-guided High-Dose-Rate (HDR) brachytherapy according to Groupe Européen de Curiethérapie and the European Society for Radiotherapy & Oncology's (GEC-ESTRO) recommendation, the patient must be transferred from room to room in order to perform 3D image guidance and HDR brachytherapy [16-18]. These fractional treatments can cause applicator displacement (uncertainties ±5.0 mm below range) that result in an approximate 5% dose-volume error to both target volume and organ at risk (OAR) for each 1 mm error. In addition, substantial changes in the DVH parameters and outliers

of up to 12 mm were observed [16, 18, 21, 22]. The reproducibility of the applicator position during inter-fraction treatments was of the utmost importance for accurate dose delivery. Therefore, one of the challenges still faced when using a brachytherapy boost is applicator displacement from the precise area on or within the body of the patient [22].

It is important to note that most of the uncertainties are unknown. For that reason, robust optimization may provide a suitable method of accounting for uncertainty. There were many ways to deal with this uncertainty [23-30]; the most straightforward approach was to predict the worst-case objective value from all scenarios and minimize their dose errors [27]. The worst scenario of maximum and minimum value could be an extreme outlier due to random variation. Typically, an extreme outlier can affect the mean of a data set but has little effect on the median. Moreover, the median absolute deviation (MAD) was more resilient to outliers in a worst-case scenario setting than the standard deviation as a robust estimator. MAD is a measure of statistical dispersion [31]. To cope with the influence of an outlier, a MAD robust estimator was applied to design a robust optimization framework in this study.

However, in real-world optimization problems, objectives are conflicting, and it cannot be a single solution [32]. Accordingly, the optimization of dwell time and dwell position using an inverse optimization technique needed to be carefully considered to improve the tumor dose coverage and reduce the dose delivered to OAR. Especially, for determination of the n dwell times at each of the n dwell positions for the desired target dose functions, a multi-objective optimization problem with complex computation [33, 34]. Classical optimization techniques are efficient at finding local minimum points; however, they may not yield the global minimum point. For solving this problem, we should search for the set of all optimal compromises. The so-called Pareto set, containing all Pareto optimal points on the basis of the objective function, has more than one local minimum. As previously mentioned, the feasible solution to a multi-objective problem in real-world optimization is to find a set of solutions. Therefore, the genetic algorithm (GA) is well suited to solve multi-objective optimization problems due to the population-based searching approach. Given the above, a preferred efficient GA that can search global minimum points as a multi-objective optimizer engine was selected to overcome the complexity of global searches [34-37].

The focus of this research was to minimize dose delivery errors due to potential applicator displacement from patient movement during cervical cancer brachytherapy treatment by using a MAD-constrained robust

optimization method with a multi-objective genetic algorithm.

2. Methods

2.A. Treatment Planning

A set of six MRI planning data sets from patients who had been previously treated with EBRT followed by cervix HDR brachytherapy were used as a representative sample in this study. A planning MRI scan was obtained with a resolution of 0.5 × 0.5 × 4 mm^3 and was completed after insertion tandem-and-ring applicators (T&R) for delivery. All patients received an EBRT dose of 50.40 Gy in 28 fractions and a BT boost dose of 25-30 Gy in 5-6 fractions. Target volume delineation, treatment planning, and dose concepts were made in accordance with the GEC-ESTRO recommendations and the EMBRACE protocol guidelines [18, 38, 39].

2.B. System Modelling

Traditionally, an optimization algorithm needs specific input data such as digitized positions, relevant anatomical structures, and a catheter to calculate a dose distribution matrix. Given the fact that we only used positional information, determining the positional characteristics of the source relative to the calculation of the point dose was completed with care.

2.B.1. Object Modelling

The contour point-lists for each structure were extracted from the DICOM-RT structure files. As each structure was represented as a set of points per single slice, it meant object shapes could be found in the MR image. Firstly, contour point-lists extracted from the DICOM images were transformed into the patient's coordinates. Next, the convex hull polygon of contour point-lists was resampled in accordance with the MRI image resolution for accurate dose calculation. Then, each resampled slice was inserted into a 3D volume, and the next set of points considered.

2.B.2. Applicator Modelling

Catheter paths were reconstructed independently with application in high-dose-rate brachytherapy. Here, MR compatible T&R applicator sets of two different sized (small and large) rings were used, each with a 30-degree angle, 2.5 mm source position separation, and with a distance from the first source to the applicator tip defined as 7 mm. The source dwell positions provided in the applicator coordinate system were defined by the applicator ring structure.

2.B.3. Source and Dose Calculation

The most widely used radioisotope source for high dose rate (HDR) brachytherapy is ^{192}Ir. The ^{192}Ir source has an actual length of 3.5 mm, enclosed within a cylindrical stainless-steel capsule with an external diameter of 1.0 mm (Figure 1). It was loaded by a remote-controlled after-loading system. AAPM TG-43 [40-42] recommended the following formalism for brachytherapy dose calculation using the ^{192}Ir source:

$$\dot{D}(r,\ \theta) = S_k \Lambda_X \frac{G_X(r,\theta)}{G_X(r_0,\theta_0)} g_X(r) F_X(r,\ \theta) \quad (1)$$

Where dosimetry parameters, S_k is the air kerma strength, Λ_X is the dose rate constant, $G_X(r,\ \theta)$ is the geometry function, $g_X(r)$ is the radial dose function, and $F_X(r,\ \theta)$ is the anisotropy function and parameter units r [cm], θ [degrees].

The geometry function is served to account for the inverse square law for point sources, $G_X(r,\ \theta)$ is calculated relative to the value on the source transverse plane ($\theta_0 = 90°$) at $r_0 = 1$cm. The radial dose function included dose fall-off from the effect of scatter and attenuation but excluded the inverse square-law correction. The anisotropy function represented the variation in dose as a function of polar angle relative to the transverse plane and described the anisotropy due to attenuation within the source.

2.C. Robust Formulation Concepts

2.C.1. Conventional Treatment Plan Optimization

We consider robust optimization for EBRT combined with HDR-BT on the minimization of the sum of functions $f_1, \ldots, f_n$. Each treatment plan quality was mathematically defined via an objective function f_k to an

anatomical structure and was minimized with respect to some decision variables x (dwell times) and $\chi \subseteq \mathbb{R}^n$ (the certain feasible set). D_{ij} was the dose deposition coefficient matrix that voxel i received per unit activity of source at dwell position j. $\mathcal{V}$ was the set of all voxels inside each contoured structure k under consideration, $\mathcal{T}$ was the set of all dwell positions, and $\mathcal{K}$ was the set of all contoured structures. $c(x;\, u)$ were the constraints to model the impact of the uncertainty of the design, u was the uncertain parameter, and $\mathcal{U}(x)$ was the set of uncertainty. We formulated the dose distribution matrix of the robust optimization problem for EBRT combined with HDR-BT as follows:

$$\begin{aligned} \underset{x\in\chi}{\text{minimize}} \quad & \sum_{k=1}^{n} f_k(d(x;u)) \\ \text{subject to} \quad & d_i = \sum_j D_{ij}x_j \qquad \forall_i \in \mathcal{V},\ \forall_j \in \mathcal{T} \\ & c(x;\, u) \geq 0 \qquad \forall_u \in \mathcal{U}(x) \end{aligned} \tag{2}$$

The voxel dose was calculated as $d_i = \sum_j D_{ij}x_j$ with dose deposition coefficient matrix and dwell times at j dwell positions. In this formula, the tradeoffs related to robustness against the uncertainty across a variety of scenarios was important in order to maximize the dose quality or minimize the error during optimization. If $\mathcal{U}(x)$ was empty for all $x \in \chi$, then the optimization could be a nominal problem.

2.C.2. Types of Uncertainty

3D image-based treatment planning with CT or MRI guidance enabled accurate target definition and dose shaping for cervical cancer. However, there were always dosimetric uncertainties where the actual dose delivered was different, for a variety of reasons. The priority ranking of the uncertainties was as follows [43]:

1. Uncertainty in dose delivery, including registration of applicator geometry to anatomy (systematic geometry variations).

2. Random inter-fraction variations gave rise to a large systematic error, such as significant variations in lung, liver, and rectum.

In this study, we were primarily focused on both systematic geometry variations and random inter-fraction variation in each fraction treatment that may give rise to a large applicator displacement. Specifically, repeated applicator insertion during HDR-BT leads to applicator position uncertainty. Consequentially, dosimetric changes occurred in both the target volume and OAR due to applicator shift (i.e., over- or underestimation of doses

delivered to the target volume and OAR) [16, 18, 21, 22]. For this study, robust optimization applied to applicator positional uncertainty.

2.C.3. Multi-objective and -criteria Robust Method

We formulated the multi-criteria robust optimization problem with uncertainty to maximize the fraction of the target volume receiving at least the prescribed dose and to minimize the maximum dose to OAR.

2.C.3.1. Worst-case Optimization Approach

The concept of the worst-case optimization optimized the maximum of each optimization function in the worst case for all scenarios. Given a dose deposition coefficient matrix $\mathrm{D_{ij}}$ (equation 2), the different dose deposition coefficient matrix under that applicator position uncertainty scenarios s denoted by $\mathrm{D_{ij}^{s}}$. Let $\mathcal{S}$ be the set of all applicator position uncertainty under consideration, then for all scenarios be the $s \in \mathcal{S}$, and all possible dose distributions $\mathrm{d_i^s}$ [27]. In addition, the constraint functions $g\big(d(x;s)\big)$ are scalar functions, and b_p are bounds on the values of constraint functions [30]. It can be formulated as:

$$\begin{aligned} \underset{x\in\chi}{\text{minimize}} \quad & \sum_{k=1}^{n} \max_{s\in\mathcal{S}} f_k(d(x;s)) \\ \text{subject to} \quad & \mathrm{d_i^s} = \sum_{j\in\mathcal{T}} \mathrm{D_{ij}^s} x_j \qquad \forall_i \in \mathcal{V},\ \forall_j \in \mathcal{T},\ \forall_s \in \mathcal{S}(x) \\ & x_j \geq 0 \\ & g\big(d(x;s)\big) \leq b_p \qquad for\ b = 1, 2, \ldots, P \end{aligned} \tag{3}$$

As mentioned above, the objective function f_k was to minimize the daily treatment uncertainty for each contoured structure. To account for errors in applicator position, we assumed that the nominal scenario was the treatment plan without considering the shifting position of the applicator (i.e., uncertainty near zero, s = 0). Notice also that displacement of applicators occurs in any direction of the patient coordinate system, ranging from -5.0 to +5.0 mm [22].

2.C.3.2. Median Absolute Deviation and Dose Volume Histogram (MAD and DVH) Constraint

Accumulate DVHs were the most effective way to describe dose distribution within the target volume or an OAR and is simply referred to as DVH. A DVH displays the percentage of the structure receiving at least a certain

dose (i.e., dose covering 90% and 98% of the high-risk clinical target volume (HRCTV), D90, and D98, according to the GEC-ESTRO recommendations). A DVH of the target volumes and OAR for each dose distribution were calculated in all applicator displacement scenarios. DVH parameter function is given by:

$$E[DVH(d)] = \sum_{i \in \mathcal{V}} P[d_i \geq d] v_i, \forall_i \in \mathcal{V} \quad (4)$$

Where d was the dose in Gy, i indexed the voxels in a given ROI, v_i was the volume of voxel i. Considering Bernoulli random variable, $d_i \geq d$ returns 0 or 1 value [44].

Trofimov et al. [45] proposed to use the DVH bands to visualize the range of DVH variation under uncertainties. Although an extreme outlier could affect the mean and standard deviation of the data, the median and MAD of the data were less liable to an extreme outlier. For that reason, we considered MAD constraint for DVH variation under uncertainties. The median and MAD functions are as follows:

$$\tilde{\lambda} = median\{DVH_s\}, \forall_s \in \mathcal{S}(x), \forall_i \in \mathcal{V} \quad (5)$$

$$MAD = b \times median\{|DVH_s - \tilde{\lambda}|\}, \forall_s \in \mathcal{S}(x), \forall_i \in \mathcal{V} \quad (6)$$

Where $\tilde{\lambda}$ was the median value of the DVH curve in a given region of interest (ROI) under uncertainties, DVH_s, and b were a constant linked to the assumption of the normality of the data, disregarding the abnormality induced by outliers, $b = 1.4826$. To control the overshot and undershot to the target volume, we used the MAD function. Using the MAD function as a selection criterion served to protect against the potentially large noise in the uncertainties data [31].

2.C.4. Multi-objective Genetic Algorithm Optimizer

In real-world applications, most of the optimization problems involve more than one objective to be optimized simultaneously. This being so, objectives may conflict with each other. A feasible solution to a multi-objective problem was to find a set of solutions. The GAs were well suited to solve multi-objective optimization problems due to a population-based searching approach. The GAs used randomized search optimization techniques inspired by natural evolution, and it used two operators to randomly generate new solutions through variation: crossover and mutation operators. The crossover operator was performed to exchange parts of two subdivisions for each

parent chromosome generated with a certain crossover probability (P_C , $i.e., break\ points$). Meanwhile, the mutation operator allowed the exchange of the positions of genes with a certain mutation probability (P_M) at two randomly chosen mutation points in a single chromosome. The crossover operator may help the convergence of the population by making the chromosomes alike, and the mutation operator was used to introduce genetic diversity back into the population. After that, the selection was made based on crowding distance. Finally, these selected candidates were then passed on to the next generation. Then, the algorithm proceeds to improve the population through repetitive operations of operators [46-48].

In this study, given an n-dimensional decision variable vector of dwell times $\mathrm{x} = \{x_1, \ldots, x_n\}$ in the solution space $\mathcal{X}$, as mentioned above, decision variable vector x was called a chromosome. Normally, the first generation of a chromosome is created randomly and called the initial population. Random generate initial values that were used when solving the problem in this work. To find a vector x^* that maximized or minimized a given set of k objectives functions $\mathrm{F}(x^*) = \{f_1(x^*), \ldots, f_k(x^*)\}$, we generated the fitness function that minimized the given objective functions and constraints for our purpose:

$$\min_{x \in \chi} f_{TARGET} = \frac{1}{N_{TARGET}} \sum_{i \in \mathcal{V}} (d_i - P_{TARGET})^2$$

$$\min_{x \in \chi} f_{OAR} = \frac{1}{N_{OAR}} \sum_{i \in \mathcal{V}} H(d_i - P_{OAR})\,(d_i - P_{OAR})^2$$

$$\min_{x \in \chi} f_{MAD} = b \times median\{|DVH_s - \tilde{\lambda}|\} \tag{7}$$

Where f_{TARGET}, f_{OAR} were objective functions for all contoured organs, and P was the prescription dose of the target volume and OAR. f_{MAD} was a MAD function of DVHs of target volume and OAR under uncertainty, and b was a fudge factor that made the MAD values equivalent to the values of standard deviation, $\mathrm{b} = 1.4826$, as previously mentioned above. Then, the constraints of the problem was given by:

$$\mathrm{d}_\mathrm{i}^s = \sum_{j \in \mathcal{T}} \mathrm{D}_{\mathrm{ij}}^s x_j \qquad \forall_i \in \mathcal{V},\ \forall_j \in \mathcal{T},\ \forall_s \in \mathcal{S}$$

$$x_j \geq 0$$

Algorithm 1 MAD-constrained robust optimization method with multi-objective genetic algorithm pseudocode

MAD-GA (*x, Fitness,* P_C, P_m)
x: population size
Fitness: determines the quality of solutions
P_C : crossover rate
P_m: mutation rate
1: *Initialise population*: $\mathcal{X}$ ← *Generate x individuals (candidate solutions) at random*
2: *Evaluate*: for each k **in** $\mathcal{X}$, calculate *Fitness(k),* check *constraints violation*
· *MAD function*: $b \times median\{|DVH_s - \tilde{\lambda}|\}$
· *EMBRACE protocol guidelines functions*
3: Realize the non-dominated population sorting
4: **while** termination criterion is not met (*stopping criteria*)
5: $\mathcal{X}_g$ ← *Create new population for generation* g
(a) *Sorting*: sort the solutions in the in ascending order
(b) *Assign*: crowding distance
(c) *Select*: tournament selection, individuals for the next generation
· Perform *crossover* between a pair of selected of individuals according to P_c
· Perform *mutation* on a selected individual according to P_m
6: *Update*: $\mathcal{X} \leftarrow \mathcal{X}_g$
7: *Evaluate*: **for each** k **in** $\mathcal{X}$, calculate *Fitness(k)*
· *MAD function, EMBRACE protocol guidelines functions*
8: **end while**
9: **Return** the individual with the highest fitness from $\mathcal{X}$

$$\mathrm{H}(d_i - P_{OAR}) = \begin{cases} 1, & d_i > P_{OAR} \\ 0, & d_i \le P_{OAR} \end{cases}$$

$$DVH_{TARGET}(x) \ge P_{TARGET}$$

$$DVH_{OAR}(x) \le P_{OAR}$$

$$\tilde{\lambda} = median\{DVH_s(\mathrm{d}_\mathrm{i}^s)\} \qquad \forall_s \in \mathcal{S}(x), \forall_i \in \mathcal{V} \qquad (8)$$

Where, $\mathrm{H}(d_i - P_{OAR})$ was the step function defined as $\mathrm{H}(d_i - P_{OAR}) = 1$ when $d_i > P_{OAR}$, otherwise $\mathrm{H}(d_i - P_{OAR}) = 0$ $(d_i \le P_{OAR})$. The DVHs of target volume and OAR were controlled with each organ's prescription dose, in accordance with the EMBRACE protocol guidelines as a constraint, respectively. Robust optimization was performed by calculating the median dose and MAD of the worst-case dose distribution and minimized these errors in each generation (Algorithm 1).

3. RESULTS

We have demonstrated what occurs on the curve of the DVH when applicator displacement occurs, and then, the performance of the robust algorithm on generating random sets of applicator displacements in any direction. Finally, we compared the treatment plan between nominal and robust methods.

3.A. DVH Variation Under Uncertainty

We investigated how DVH curves were changed according to uncertainty in dose delivery by applicator geometry to OARs. With the assumption that the applicator moves randomly in any direction (±5.0 mm below range x, y, and z), the dose variation from applicator positional errors for each target and organ has been plotted (figure 1). We only considered a total of 80 scenarios within a nominal scenario (figure 1) that were chosen randomly.

3.B. Performance of the Robust Algorithm

Figures 2 and 3 illustrate the comparison of iso-dose lines of nominal (manual) planning, inverse planning, and robust planning for a cervical cancer patient who was treated with an EBRT total dose 5040 cGy, delivered in 28 fractions with an ICR total dose of 3000 cGy delivered in five fractions using a T&R applicator. The yellow arrow with a single arrowhead represents the overlap region between the bladder (dark blue color dot line) and TG43 iso-dose line. In all planning, dwell time at each position for desired target coverage was optimized by the previously mentioned three methods. For all planning, the prescription iso-dose line was successfully encompassed based on EMBRACE protocol guidance. As shown in figure 2, we can identify that bladder contour is encompassed by a minimum of percent iso-dose line in the robust planning while maintaining adequate target dose coverage and OAR sparing, rather than both coverage and sparing in the nominal and inverse planning. In figure 3, the cervix brachytherapy plan illustrated the iso-dose line on a coronal view. Figure 3 demonstrated a reduced dose to the ICRU vaginal R, L point, and sigmoid than nominal and inverse planning (blue arrow with a single arrowhead). Furthermore, the robust planning not only minimizes the dose delivery of the ICRU vaginal R and L point, it minimized the doses to the OAR, too, while maintaining coverage of uneven high risk and

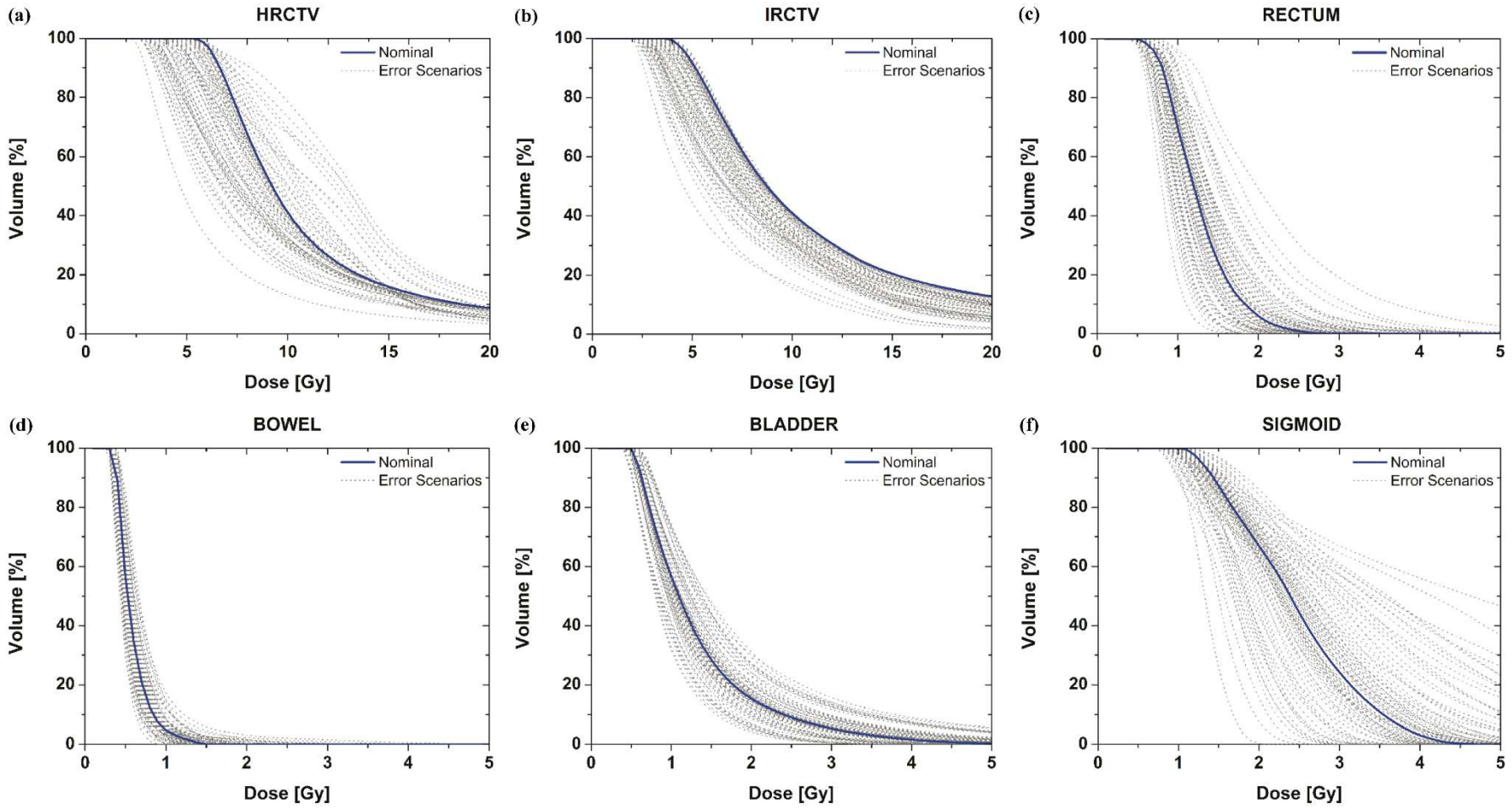

275 **Figure 1.** DVH curve variation of the targets (a)-(b) and OAR (c)-(f) under applicator positional errors with the assumption of shift scenarios. The DVH for the nominal

276 (expected) plan is in blue, and the DVHs for 79 error scenarios are in grey.

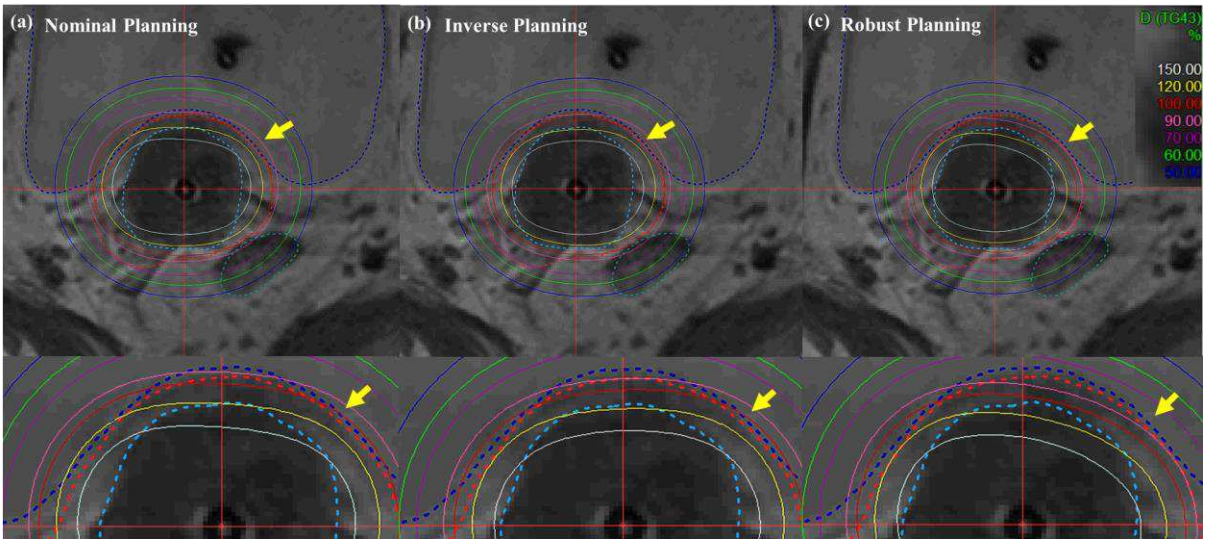

Figure 2. Iso-dose line comparison of (a) nominal (manual) planning, (b) inverse planning, and (c) robust planning standard planning in EBRT-BT boost treatment of cervical cancer: axial view. An EBRT total dose of 5040 cGy was delivered in 28 fractions, and an ICR total dose of 3000 cGy was delivered in 6 fractions using a T&R applicator.

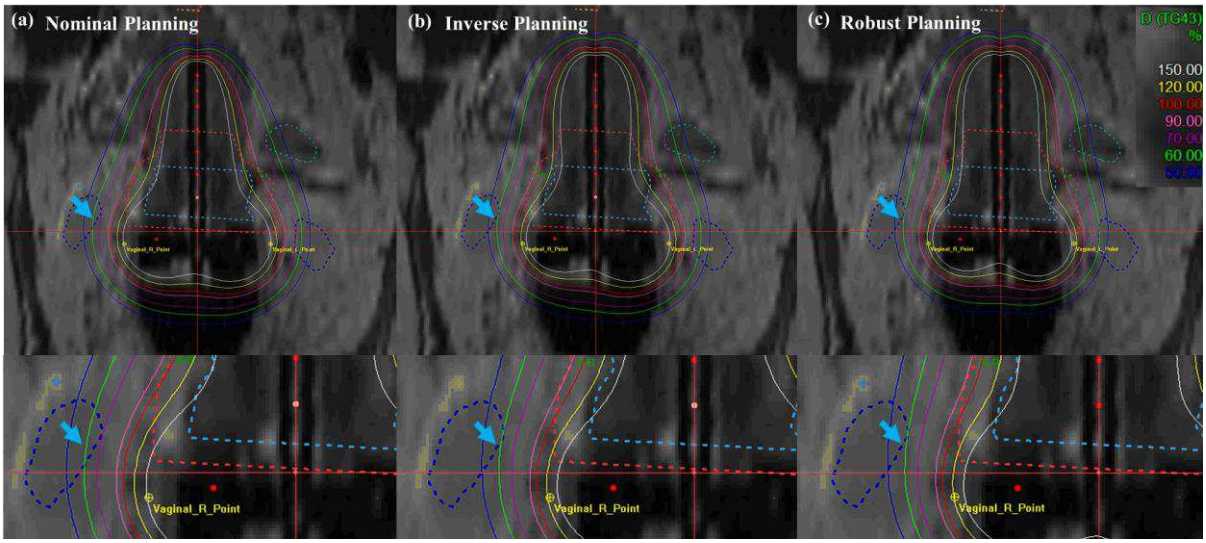

Figure 3. Iso-dose line comparison of (a) nominal (manual) planning, (b) inverse planning, and (c) robust planning standard planning in EBRT-BT boost treatment of cervical cancer: coronal view. An EBRT total dose of 5040 cGy was delivered in 28 fractions, and an ICR total dose of 3000 cGy was delivered in 6 fractions using a T&R applicator.

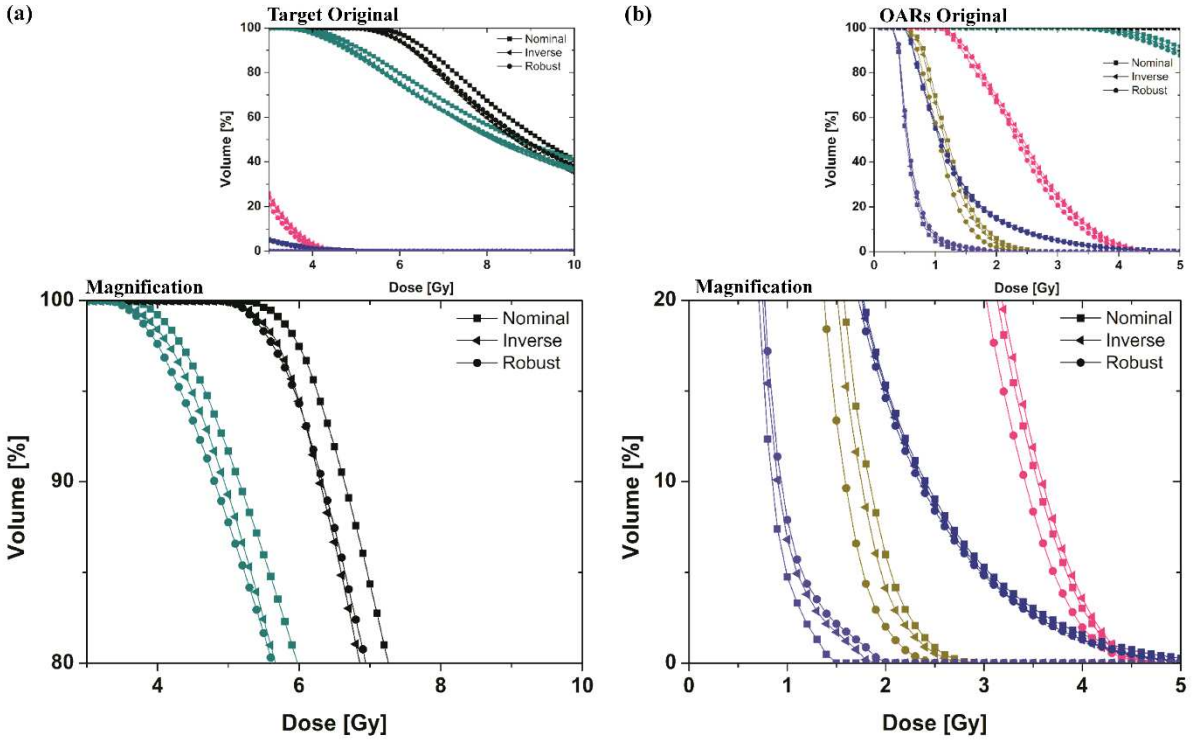

Figure 4. DVH curves for nominal (manual) planning, inverse planning, and robust planning in EBRT-BT boost treatment of cervical cancer were plotted using colors indicating: HRCTV-Black, IRCTV-Dark Cyan, Rectum-Dark Yellow, Sigmoid-Pink, Bladder-Royal, Bowel-Violet. Graphs (a) and (b) are the magnification of the DVH curves of the target and OAR.

intermediate-risk CTV (HR and IRCTV) contour.

In addition, the effect of robust optimization with MAD-constrained concepts was demonstrated in figure 4, 5, and table 1. Figure 4 illustrates the DVH curves from the nominal, inverse, and robust planning for EBRT-BT boost treatment of cervical cancer. The target receives a sufficient dose in all plans, furthermore, improved rectal, sigmoid, bladder, and bowel dose sparing. We found no significant violation of EMBRACE protocol guidance in any DVH parameters of the target volume or OAR using the robust planning.

Table 1 displays the numerical results corresponding to figures 2 and 3. Quantitative results in table 1 indicated the differences in equivalent doses in 2 Gy fractions (EQD2) and standard deviation. Our treatment, a total dose of 50.40 Gy to the target, was delivered by EBRT. The EQD2 of HRCTV D98 for all plans (nominal, inverse, and

Table 1. The dose constraints in accordance with EMBRACE recommendation and the total EQD2 (EBRT + BT) of each target and OAR for nominal, inverse and robust plan strategy.

EQD2 and standard deviation of dose distributions				
	EMBRACE Recommendation*	**Nominal Plan EQD2 (σ_{BT})**	**Inverse Plan EQD2 (σ_{BT})**	**Robust Plan EQD2 (σ_{BT})**
Target	$\alpha/\beta = 10\ Gy$			
HRCTV	D98 $> 75^*$	85.59 ($\pm$1.0177)	86.71 ($\pm$0.9393)	84.84 ($\pm$0.9085)
	D90 $> 90^*$	92.15 ($\pm$1.884)	92.63 ($\pm$0.10983)	91.56 ($\pm$1.0341)
IRCTV	D98 $> 60^*$	74.96 ($\pm$0.6424)	73.29 ($\pm$0.6063)	72.24 ($\pm$0.5883)
	D90 $> 66^*$	82.18 ($\pm$0.7418)	80.66 ($\pm$0.6927)	78.83 ($\pm$0.6737)
OAR	$\alpha/\beta = 3\ Gy$			
Rectum	$D_{2cc} < 75^*$	55.29 ($\pm$0.4927)	54.94 ($\pm$0.4620)	54.09 ($\pm$0.4052)
Sigmoid	$D_{2cc} < 75^*$	68.20 ($\pm$1.2491)	69.13 ($\pm$1.2718)	67.25 ($\pm$1.1199)
Bladder	$D_{2cc} < 90^*$	84.98 ($\pm$2.1211)	81.25 ($\pm$1.9764)	81.35 ($\pm$2.1459)
Bowel	$D_{2cc} < 60^*$	51.06 ($\pm$0.1864)	51.41 ($\pm$0.2270)	51.58 ($\pm$0.2474)

robust planning) was estimated at 85.59 Gy_{EQD2}, 86.71 Gy_{EQD2}, and 84.84 Gy_{EQD2}, respectively, and the standard deviations for each plan were ±1.0177, ±0.9393 and ±0.9085, respectively. Also, the EQD2 and standard deviation of the rectum $D_{2cc} < 75^*$ for all plans were also estimated at 55.29 Gy_{EQD2} (±0.4927), 54.94 Gy_{EQD2} (±0.4620) and 54.09 Gy_{EQD2} (±0.4052), respectively. Robust planning standard deviations were less than other strategies in both HRCTV and rectum. In this case, in order to show the different dose variations between nominal and robust planning, DVH curves with error scenarios for target and OAR were plotted using colors (figure 5). Moreover, although both plans satisfied the requirements for the prescription dose coverage of the target and OAR, the band width of robust DVH curves with error scenarios in all organs were much thinner than the DVHs of the nominal plan.

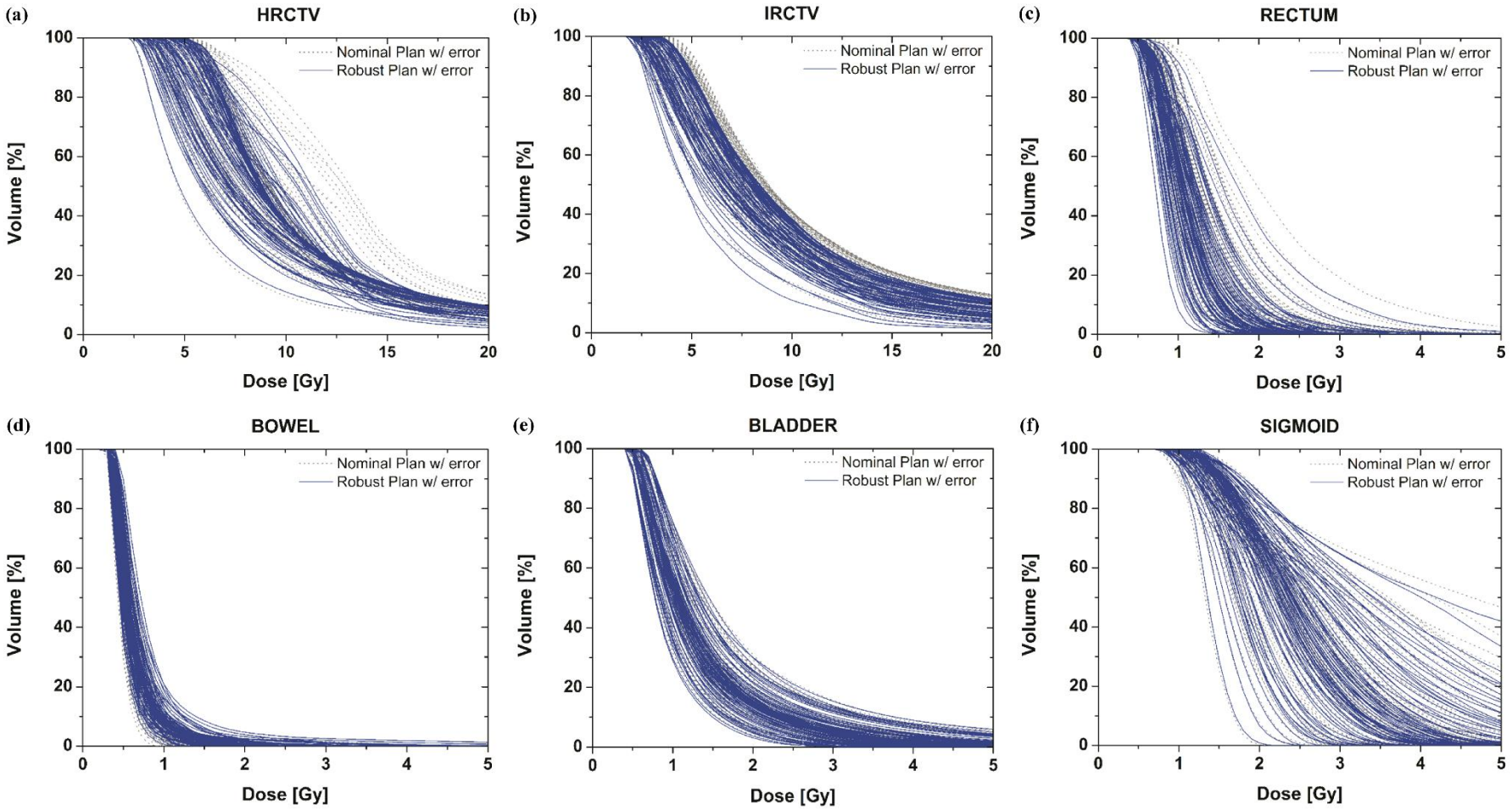

312 **Figure 5.** DVH curve variation of the targets (a)-(b) and OAR (c)-(f) under applicator positional errors with the shift scenario assumptions. DVHs from the robust, optimized

313 plan with error scenarios are shown using a straight blue line, and the nominal DVHs of the non-robust plan with error scenarios are indicated by the grey dotted lines.

314 **Table 2.** Evaluation of five case sets for nominal and robust plans in the EBRT-BT boost.

EQD2 and standard deviation of dose distributions						
	EMBRACE Recommendation *		Nominal Plan		Robust Plan	
			EQD2	(σ_{BT})	EQD2	(σ_{BT})
Case 1	HRCTV	D98 $> 75^*$	84.03	$\pm$0.4639	83.59	$\pm$0.4483
		D90 $> 90^*$	90.13	$\pm$0.4629	90.01	$\pm$0.4379
	IRCTV	D98 $> 75^*$	67.22	$\pm$0.3097	67.23	$\pm$0.3008
		D90 $> 90^*$	72.55	$\pm$0.3019	72.76	$\pm$0.3145
	Rectum	$D_{2cc} < 75^*$	51.96	$\pm$0.0516	52.01	$\pm$0.0553
	Sigmoid	$D_{2cc} < 75^*$	62.30	$\pm$0.4959	62.99	$\pm$0.4938
	Bladder	$D_{2cc} < 90^*$	82.58	$\pm$0.2123	81.66	$\pm$0.2087
	Bowel	$D_{2cc} < 60^*$	59.84	$\pm$0.1928	59.61	$\pm$0.1857
Case 2	HRCTV	D98 $> 75^*$	79.31	$\pm$0.4338	78.22	$\pm$0.4391
		D90 $> 90^*$	90.03	$\pm$0.3820	90.28	$\pm$0.5147
	IRCTV	D98 $> 75^*$	66.05	$\pm$0.2952	64.32	$\pm$0.2921
		D90 $> 90^*$	73.49	$\pm$0.3505	71.77	$\pm$0.3533
	Rectum	$D_{2cc} < 75^*$	79.26	$\pm$0.4317	83.42	$\pm$0.5736
	Sigmoid	$D_{2cc} < 75^*$	73.26	$\pm$0.5294	70.57	$\pm$0.2927
	Bladder	$D_{2cc} < 90^*$	83.01	$\pm$0.2235	78.39	$\pm$0.5568
	Bowel	$D_{2cc} < 60^*$	62.16	$\pm$0.2225	58.57	$\pm$0.1755
Case 3	HRCTV	D98 $> 75^*$	92.17	$\pm$0.6438	83.71	$\pm$0.5736
		D90 $> 90^*$	98.85	$\pm$0.6284	90.15	$\pm$0.5880
	IRCTV	D98 $> 75^*$	72.85	$\pm$0.2978	70.19	$\pm$0.3018
		D90 $> 90^*$	79.36	$\pm$0.3139	76.00	$\pm$0.3151
	Rectum	$D_{2cc} < 75^*$	74.46	$\pm$0.6353	71.61	$\pm$0.6344
	Sigmoid	$D_{2cc} < 75^*$	74.66	$\pm$1.0074	69.57	$\pm$0.6055
	Bladder	$D_{2cc} < 90^*$	86.29	$\pm$0.2854	81.09	$\pm$0.7346
	Bowel	$D_{2cc} < 60^*$	54.36	$\pm$0.1325	53.31	$\pm$0.0926
Case 4	HRCTV	D98 $> 75^*$	89.25	$\pm$0.6313	88.66	$\pm$0.6478
		D90 $> 90^*$	97.17	$\pm$0.6561	97.13	$\pm$0.6669
	IRCTV	D98 $> 75^*$	71.25	$\pm$0.2754	70.91	$\pm$0.2825
		D90 $> 90^*$	80.26	$\pm$0.3128	79.95	$\pm$0.3240
	Rectum	$D_{2cc} < 75^*$	60.99	$\pm$0.2183	60.66	$\pm$0.2138
	Sigmoid	$D_{2cc} < 75^*$	78.21	$\pm$0.8241	78.01	$\pm$0.6318
	Bladder	$D_{2cc} < 90^*$	92.09	$\pm$0.6173	91.98	$\pm$0.8922
	Bowel	$D_{2cc} < 60^*$	52.14	$\pm$0.0566	52.26	$\pm$0.0563

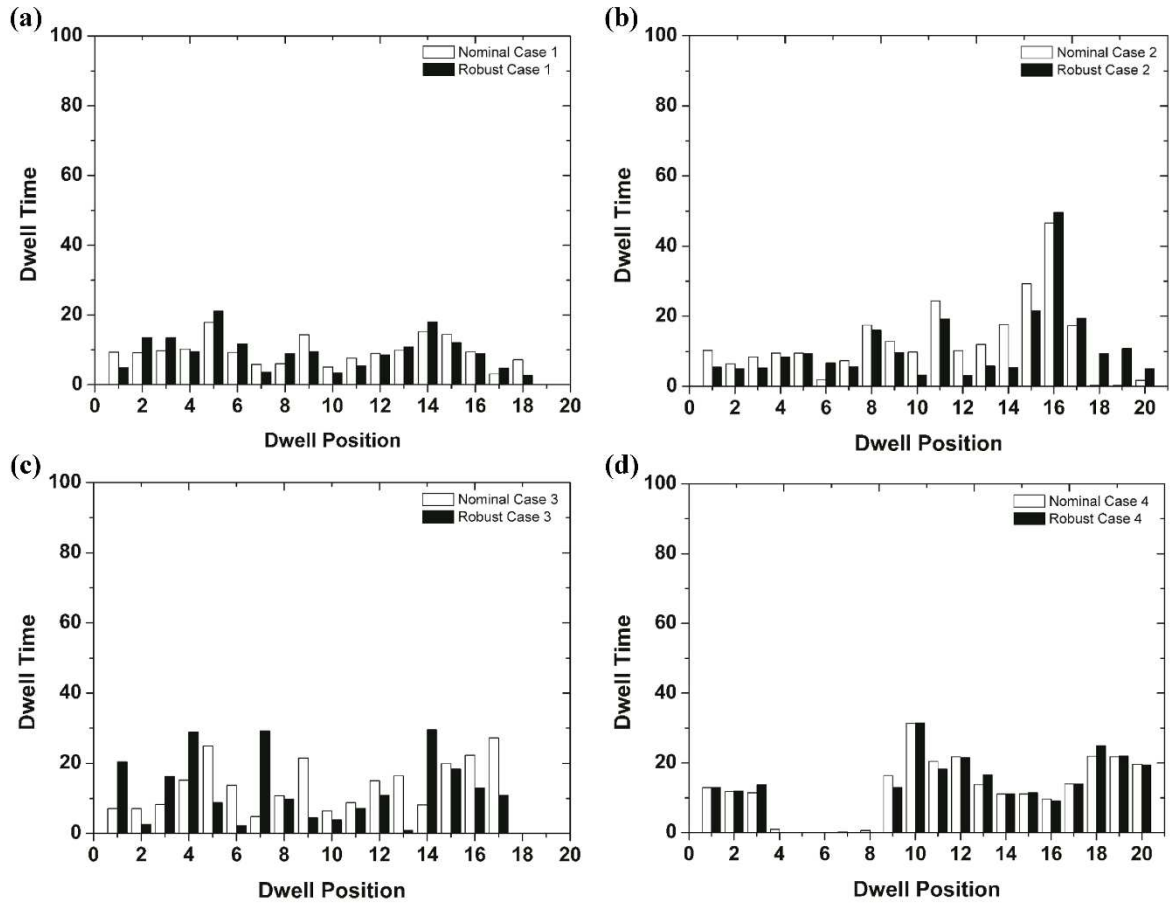

Figure 6. Distribution of dwell times along the tandem and ring applicators in four cases with robust planning. The corresponding dwell times for a manual optimization (nominal) is also presented for comparison: (a) case 1, (b) case 2, (c) case 3 and (d) case 4 are the each plan comparisons of distribution of dwell times.

3.C. Evaluation of Robust Algorithm with Four Case Sets

Further evaluation of our robust strategy compared the plan robustness in the nominal and robust plans (table 2). The prepared four case sets of applicator positional errors can be divided into two categories. Two cases (cases 2 and 4) were challenging to fit with the EMBRACE protocol guidance, but the other two cases (cases 1 and 3) were a better fit. Table 2 shows the comparison of the EQD2 and the standard deviation values of each strategy. As the above results, this robust strategy could also reduce the standard deviation of target and OAR compared to the nominal plan in most of the cases, whereas the standard deviation of a few organs was not promising. However, the dose delivered results of EQD2 from all cases were optimized delivered doses and also satisfied the

EMBRACE protocol guidance related to the target and OAR. Moreover, although the standard deviation in a few organs was not sufficiently minimized, the resulted robustness plans from our strategy might be worth considering according to EMBRACE protocol guidance. In addition, figure 6 demonstrated relative dwell time differences in each case. In the summation of total dwell times, there was not much difference between the two nominal and robust plans. However, we may determine dose differences from the above results.

4. DISCUSSION

We would like to emphasize that applicator displacement during brachytherapy treatment for cervical cancer lead to radical changes in dose distribution [49]. With the advent of MRI guided EBRT-BT, the opportunity to improve outcomes by increasing the dose while minimizing the dose to OAR is essential in the management of locally advanced cervical cancer. Hence, the applicator displacement uncertainty is of significant relevance within the distribution of dose prescription. Many studies have demonstrated that applicator displacement is a problem of critical importance.

Joshua et al. [22] quantified the dosimetric impact of applicator displacements and applicator reconstruction-uncertainties through simulated planning studies of virtual applicator shifts. In addition, Tanderup et al. [21] reported 2 mm errors in applicator reconstruction. However, the reconstruction approach was rather limited due to the finite slice thickness, resulting in several sources of uncertainty. Junyi et al. [24] developed a real-time applicator position monitoring system with a 1 mm accuracy during long wait times between imaging and treatment. Nevertheless, the real-time monitoring system still depends on the accuracy of distance computability between the camera and marker.

Furthermore, applicator shifting and organ movement are inevitable, and it leads to errors in the fractional dose delivery. De Leeuw et al. [16] found geometrical shifts as large as 6 ± 7 mm in the posterior direction. Several studies have previously reported such movements relative to target and organs [16-18, 23]. While these efforts may reduce required dose delivery and errors, there will always remain residual uncertainties.

As mentioned in the above sections, the extreme outlier of the DVH parameter due to random applicator shifting could have occurred. The incorporation of random applicator shifting uncertainty into the robust optimization with

the utilization of MAD function enabled the genetic algorithm approach to minimize the extreme outlier. Hence, a robust optimization method with a multi-objective genetic algorithm approach for minimizing dose delivery errors by potential applicator displacement was proposed. Instead of using mean and standard constraints for extreme standard deviations in these scenarios, the MAD function could have found the optimum less affected by outliers.

We demonstrated the feasibility of using our robust optimization strategy to minimize potential applicator positional errors with dose delivery variations. The dwell positions and times were determined in a way that mathematically improved the plan quality according to GEC-ESTRO Working Group recommendations. Compared to manual plan approaches, our method resulted in a reduced standard deviation on DVH parameters while maintaining the target dose coverage and sparing OAR. In the complex plan case, we should consider a weighted parameter for each organ to deal with exceptional cases such as overshot and undershot of the target and OAR.

Nonetheless, one advantage of the proposed method is that it functions in a similar way to a deep learning approach with given multi-constraints and -objective functions. In addition, it has the ability to avoid being trapped in local optimal solution by searching parallel from a population of points. However, multi-objective function evaluations are often highly time-consuming. Hence, our robust algorithm needs to be used in conjunction with a graphics processing unit (GPU) accelerator to evaluate objective functions and to calculate the dose matrix for each generation. In the future, we aim to develop the proposed in-house accelerating software.

5. CONCLUSION

Here, we have proposed a robust optimization method with a multi-objective, genetic-algorithm approach using MAD and DVH parameter constraints for minimizing dose delivery errors by potential applicator displacement. The fundamental assumption that only random displacements of applicators were formulated mathematically in terms of objective functions. Subsequently, a mathematical optimization algorithm was used to minimize the objective function value to best meet the planning goals. Finally, the use of this algorithm enabled the minimization of dose delivery errors by potential applicator displacement and acceptable robustness planning.

Abbreviations

MAD: median absolute deviation; T&R: tandem and ring; MRI: Magnetic Resonance Imaging; OAR: organs at risk; EQD2: equivalent dose in 2 Gy fractions; HR-CTV: high-risk clinical target volume; D98: dose that covers 98% of the target volume; EBRT: External beam radiation therapy; BT: brachytherapy; DVH: Dose-Volume-Histogram; CT: computed tomography; HDR: High-Dose-Rate; GEC-ESTRO: Groupe Européen de Curiethérapie and the European Society for Radiotherapy & Oncology's; GA: genetic algorithm; ROI: region of interest; D_{2cc}: D2cc : doses to the volume of 2 cc in Gy.

Acknowledgment

Not applicable.

Authors' contributions

BJ and HK conceived and coordinated the study, designed, performed, and analyzed the experiments, and wrote the manuscript. BJ, KP, KHK, HJK, and HK revised the manuscript. All authors reviewed the results and approved the final version of the manuscript.

Funding

This research was supported by the National Research Foundation of Korea (NRF-2017R1D1A1B03035002) and the Korean National Cancer Center Fund (1810272-3).

Availability of data and materials

All data generated or analyzed during this study are included in this manuscript.

401 **Ethics approval and consent to participate**

402 Not applicable.

403

404 **Consent for publication**

405 Not applicable.

406

407 **Competing interests**

408 The authors declare that they have no competing interests.

409

410 **Author details**

411 [1]Department of Radiological Science, College of Health Science, Yonsei University, Wonju, Korea.

412 [2]Proton Therapy Center, National Cancer Center, Goyang, Korea

413

414 **References**

415 1. Bray F, Ferlay J, Soerjomataram I, Siegel RL, Torre LA, Jemal A. Global cancer statistics, 2018. *CA CANCER*
416 *J CLIN* 2018;68:394-424.

417 2. Kamangar F, Dores GM, Anderson WF. Patterns of cancer incidence, mortality, and prevalence across five
418 continents: Defining priorities to reduce cancer disparities in different geographic regions of the world. *J Clin*
419 Oncol 2006;24(14):2137-2150.

420 3. Liu YM, Ni LQ, Wang SS, Lv QL, Chen WJ1, Ying SP. Outcome and prognostic factors in cervical cancer
421 patients treated with surgery and concurrent chemoradiotherapy: a retrospective study. *World J Surg Oncol*
422 2018;16(1):18.

423 4. Ohara K, Sugahara S, Kagei K, Hata M, Igaki H, Tokuuye K, et al. Retrospective comparison of clinical

outcome between radiotherapy alone and surgery plus postoperative radiotherapy in the treatment of stages IBIIB cervical squamous cell carcinoma. *Radiat Med* 2004;22(1):42-8.

5. Robyn Banerjee, Mitchell Kamrava. Brachytherapy in the treatment of cervical cancer: a review. *Int J Women's Health* 2014;6:555-564.

6. Al Feghali KA, Elshaikh MA. Why brachytherapy boost is the treatment of choice for most women with locally advanced cervical carcinoma?. *Brachytherapy* 2016;15:191-199.

7. Mahmoud O, Kilic S, Khan AJ, Beriwal S, Small W Jr. External beam techniques to boost cervical cancer when brachytherapy is not an option—theories and applications. *Ann Transl Med* 2017;5(10):207.

8. Korenaga TRK, Pierson W, Swanson M, Chapman JS. Better late than never: Brachytherapy is more important than timeframe in cervical cancer outcomes [Abstracts]. *Gynecologic Oncology* 2019;154:7

9. Nikoofar A, Hoseinpour Z, Rabi Mahdavi S, Hasanzadeh H, Rezaei Tavirani M. High-Dose-Rate 192Ir Brachytherapy Dose Verification: A Phantom Study. *Iran J Cancer Prev* 2015;8(3):e2330.

10. Henschke UK. "Afterloading" applicator for radiation therapy of carcinoma of the uterus. *Radiology* 1960;74(5):834.

11. Shwetha B, Ravikumar M, Palled SR, Supe SS, Sathiyan S. Dosimetric comparison of high dose rate brachytherapy and intensity-modulated radiation therapy for cervical carcinoma. *J Med Phys* 2011;36(2): 111-116.

12. DeWerd LA, Ibbott GS, Meigooni AS, Mitch MG, Rivard MJ, Stump KE et al. A dosimetric uncertainty analysis for photon-emitting brachytherapy sources: Report of AAPM Task Group No. 138 and GEC-ESTRO. *Med Phys* 2011;38:782-801.

13. Berger D, Dimopoulos J, Georg P, Georg D, Pötter R, Kirisits C. Uncertainties in assessment of the vaginal dose for intracavitary brachytherapy of cervical cancer using a tandem-ring applicator. *Int. J. Radiation Oncology Biol. Phys* 2007;67(5):1451-1459.

14. Swamidas J, Mahantshetty U, Tanderup K, Malvankar D, Sharma S, Engineer R, et al. Inter-application variation of dose and spatial location of D_2cm^3 volumes of OARs during MR image based cervix

449 brachytherapy. *Radiother Oncol* 2013;107:58-62.

450 15. John A Vargo, Sushil Beriwal. Image-based brachytherapy for cervical cancer. *World J Clin Oncol* 2014;5(5):
451 921-930.

452 16. De Leeuw AA, Moerland MA, Nomden C, Tersteeg RH, Roesink JM, Jürgenliemk-Schulz IM. Applicator
453 reconstruction and applicator shifts in 3D MR-based PDR brachytherapy of cervical cancer. *Radiother Oncol*
454 2009;93:341-6.

455 17. Hellebust TP, Tanderup K, Bergstrand ES, Knutsen BH, Røislien J, Olsen DR. Reconstruction of a ring
456 applicator using CT imaging: impact of the reconstruction method and applicator orientation. *Phys Med Biol*
457 2007;52:4893-904.

458 18. Hellebust TP, Kirisits C, Berger D, Pérez-Calatayud J, De Brabandere M, De Leeuw A, et al.
459 Recommendations from Gynaecological (GYN) GEC-ESTRO Working Group (III): considerations and
460 pitfalls in commissioning and applicator reconstruction in 3D image-based treatment planning of cervix
461 cancer brachytherapy. *Radiother Oncol* 2010;96:153-60.

462 19. Andersen SE, Noe KØ, Sørensen TS, Nielsen SK, Fokdal L, Paludan M, et al. Simple DVH parameter
463 addition as compared to deformable registration for bladder dose accumulation in cervix cancer brachytherapy.
464 *Radiother Oncol* 2013;107(1):52-7.

465 20. Lang S, Nesvacil N, Kirisits C, Georg P, Dimopoulos JC, Federico M, et al. Uncertainty analysis for 3D
466 image-based cervix cancer brachytherapy by repetitive MR imaging: assessment of DVH variations between
467 two HDR fractions within one applicator insertion and their clinical relevance. *Radiother Oncol*
468 2013;107(1):26-31.

469 21. K. Tanderup, T.P. Hellebust, Lang S, Granfeldt J, Pötter R, Lindegaard JC, et al. Consequences of random
470 and systematic reconstruction uncertainties in 3D image based brachytherapy in cervical cancer. *Radiother*
471 *Oncol* 2008;89:156-163.

472 22. Schindel J, Zhang W, Bhatia SK, Sun W, Kim Y. Dosimetric impacts of applicator displacements and
473 applicator reconstruction uncertainties on 3D image-guided brachytherapy for cervical cancer. *J Contemp*

474 *Brachytherapy* 2013;5(4):250-7.

475 23. Oku Y, Arimura H, Nguyen TT, Hiraki Y, Toyota M, Saigo Y, et al. Investigation of whether in-room CT-
476 based adaptive intracavitary brachytherapy for uterine cervical cancer is robust against interfractional location
477 variations of organs and/or applicators. *J Radiat Res* 2016;57(6):677-683.

478 24. Junyi X, Timothy W, Kim Y. A real-time applicator position monitoring system for gynecologic intracavitary
479 brachytherapy. *Med. Phys* 2014;41(1):011703.

480 25. Webster MJ, Devic S, Vuong T, Han DY, Scanderbeg D, Choi D, et al. HDR brachytherapy of rectal cancer
481 using a novel grooved-shielding applicator design. *Med Phys* 2013;40:091704.

482 26. Fredriksson A, Bokrantz R. A critical evaluation of worst case optimization methods for robust intensity-
483 modulated proton therapy planning. *Med Phys* 2014;41(8): 081701.

484 27. Fredriksson A, A characterization of robust radiation therapy treatment planning methods—from expected
485 value to worst case optimization. *Med Phys* 2012;39(8):5169-5181.

486 28. Chu M, Zinchenko Y, Henderson SG, Sharpe MB. Robust optimization for intensity modulated radiation
487 therapy treatment planning under uncertainty. *Phys Med Biol* 2005;50(23):5463-77.

488 29. Tilly, D., Holm, Å., Grusell, E., Ahnesjö, A. Probabilistic optimization of dose coverage in radiotherapy.
489 *Physics and Imaging in Radiation Oncology* 2019;10:1-6

490 30. Chen W, Unkelbach J, Trofimov A, Madden T, Kooy H, Bortfeld T, et al. Including robustness in multi-criteria
491 optimization for intensity-modulated proton therapy. *Phys Med Biol* 2012;57(3):591-608.

492 31. Chen R, Paschalidis I. Outlier Detection Using Robust Optimization with Uncertainty Sets Constructed from
493 Risk Measures. *ACM SIGMETRICS Performance Evaluation Review* 2018;45(3):174-179.

494 32. Hu S, Wu X, Liu H, Wang Y, Li R, Yin M. Multi-Objective Neighborhood Search Algorithm Based on
495 Decomposition for Multi-Objective Minimum Weighted Vertex Cover Problem. *Sustainability* 2019;11:3634

496 33. Chiandussi G, Codegone M, Ferrero S, Varesio FE. Comparison of multi-objective optimization
497 methodologies for engineering applications. Proceedings of the Thirty-First AAAI Conference on Artificial

498 Intelligence. *Comput Math Appl* 2012;63:912-942.

499 34. Deist TM, Gorissen BL. High-dose-rate prostate brachytherapy inverse planning on dose-volume criteria by
500 simulated annealing. *Phys Med Biol* 2016;61(3):1155-1170.

501 35. Morén B1, Larsson T, Carlsson Tedgren Å. Mathematical optimization of high dose-rate brachytherapy
502 derivation of a linear penalty model from a dose-volume model. *Phys Med Biol* 2018;63(6):065011.

503 36. Ghaheri A, Shoar S, Naderan M, Hoseini SS. The Applications of Genetic Algorithms in Medicine. *Oman*
504 *Med J* 2015;30(6):406-416.

505 37. Sabbir U. Ahmad, Stuart W.A. Bergen. A genetic algorithm approach to the inverse problem of treatment
506 planning for intensity-modulated radiotherapy. *Biomed Signal Process Control* 2010;5:189-195.

507 38. Pötter R, Tanderup K, Kirisits C, de Leeuw A, Kirchheiner K, Nout R, et al. The EMBRACE II study: The
508 outcome and prospect of two decades of evolution within the GEC-ESTRO GYN working group and the
509 EMBRACE studies. *Clin Transl Radiat Oncol* 2018;9:48-60.

510 39. Sturdza A, Pötter R, Fokdal LU, Haie-Meder C, Tan LT, Mazeron R, et al. Image guided brachytherapy in
511 locally advanced cervical cancer: improved pelvic control and survival in RetroEMBRACE, a multicenter
512 cohort study. *Radiother Oncol* 2016;120(3):428-33.

513 40. Nath R, Anderson LL, Luxton G, Weaver KA, Williamson JF, Meigooni AS. Dosimetry of interstitial
514 brachytherapy sources: Recommendations of the AAPM Radiation Therapy Committee Task Group No. 43.
515 American Association of Physicists in Medicine. *Med. Phys* 1995;22:209-34.

516 41. Rivard MJ, Coursey BM, DeWerd LA, Hanson WF, Huq MS, Ibbott GS. Update of AAPM Task Group No.
517 43 Report: a revised AAPM protocol for brachytherapy dose calculations. *Med Phys* 2004;31:633-74.

518 42. Rivard MJ, Ballester F, Butler WM, DeWerd LA, Ibbott GS, Meigooni AS. Supplement to the 2004 update
519 of the AAPM Task Group No. 43 Report. *Med Phys* 2017;34:2187-2205.

520 43. Kirisits C, Rivard MJ, Baltas D, Ballester F, De Brabandere M, van der Laarse R, et al. Review of clinical
521 brachytherapy uncertainties: Analysis guidelines of GEC-ESTRO and the AAPM. *Radiother Oncol*
522 2014;110:199-212.

523 44. Park PC, Cheung JP, Zhu XR, Lee AK, Sahoo N, Tucker SL, et al. Statistical Assessment of Proton Treatment
524 Plans Under Setup and Range Uncertainties. *Int J Radiat Oncol Biol Phys*. 2013;86:1007-13.

525 45. Trofimov A, Unkelbach J, DeLaney TF, Bortfeld T. Visualization of a variety of possible dosimetric outcomes
526 in radiation therapy using dose volume histogram bands. *Pract Radiat Oncol* 2012;2:164-171.

527 46. Kalyanmoy Deb, A Fast and Elitist Multiobjective Genetic Algorithm: NSGA-II. *IEEE Transactions on*
528 *Evolutionary Computation*, 2002;6(2):182-197.

529 47. Konaka A, Coitb DW, Smith AE, Multi-objective optimization using genetic algorithms: A tutorial. *Reliab*
530 *Eng Syst Safe* 2006;91:992-1007.

531 48. Hajela P, lin CY. Genetic search strategies in multicriterion optimal design. *Struct Optimization* 1992;4(2):99-
532 107.

533 49. Tanderup K, Eifel PJ, Yashar CM, Pötter R, Grigsby PW. Curative radiation therapy for locally advanced
534 cervical cancer: brachytherapy is NOT optional. *Int J Radiat Oncol Biol Phys* 2014;88(3):537-9.

Figures

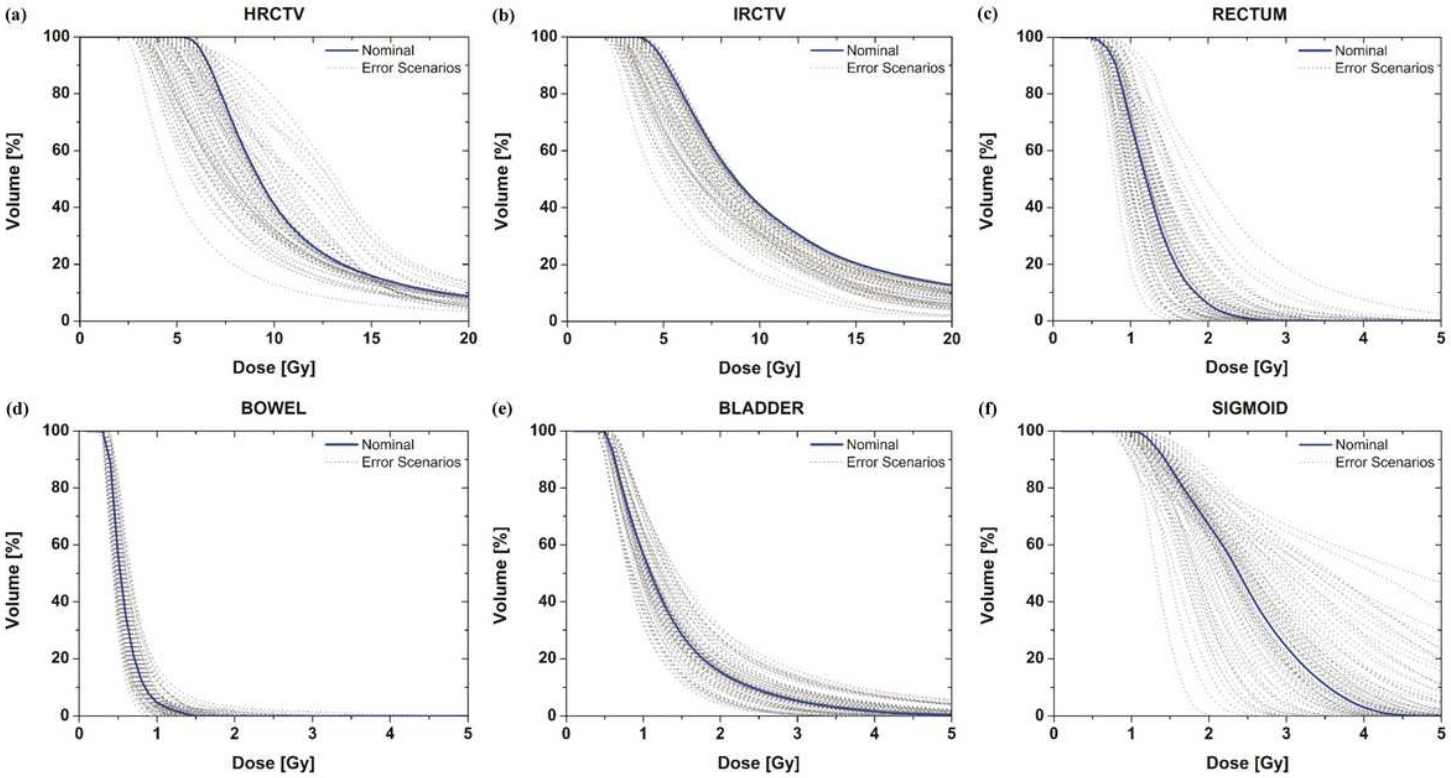

Figure 1

DVH curve variation of the targets (a)-(b) and OAR (c)-(f) under applicator positional errors with the assumption of shift scenarios. The DVH for the nominal (expected) plan is in blue, and the DVHs for 79 error scenarios are in grey.

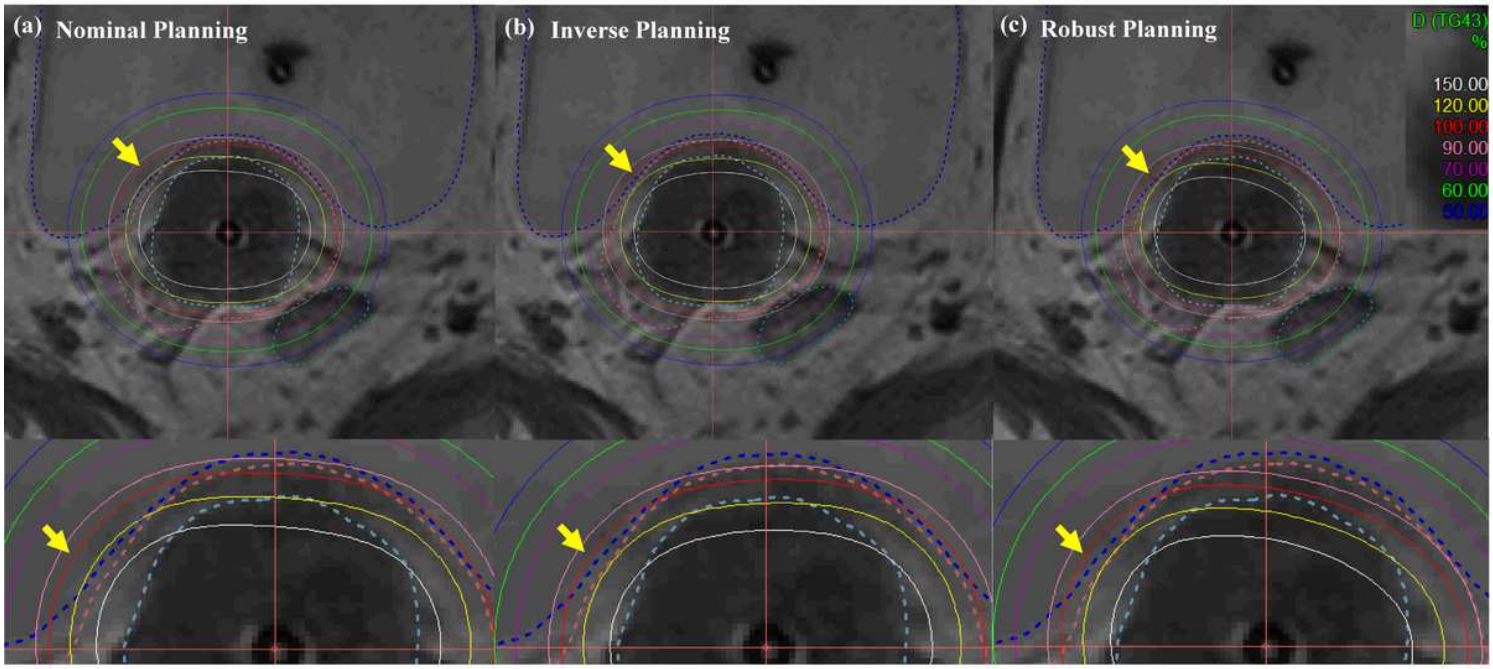

Figure 2

Iso-dose line comparison of (a) nominal (manual) planning, (b) inverse planning, and (c) robust planning standard planning in EBRT-BT boost treatment of cervical cancer: axial view. An EBRT total dose of 5040 cGy was delivered in 28 fractions, and an ICR total dose of 3000 cGy was delivered in 6 fractions using a T&R applicator.

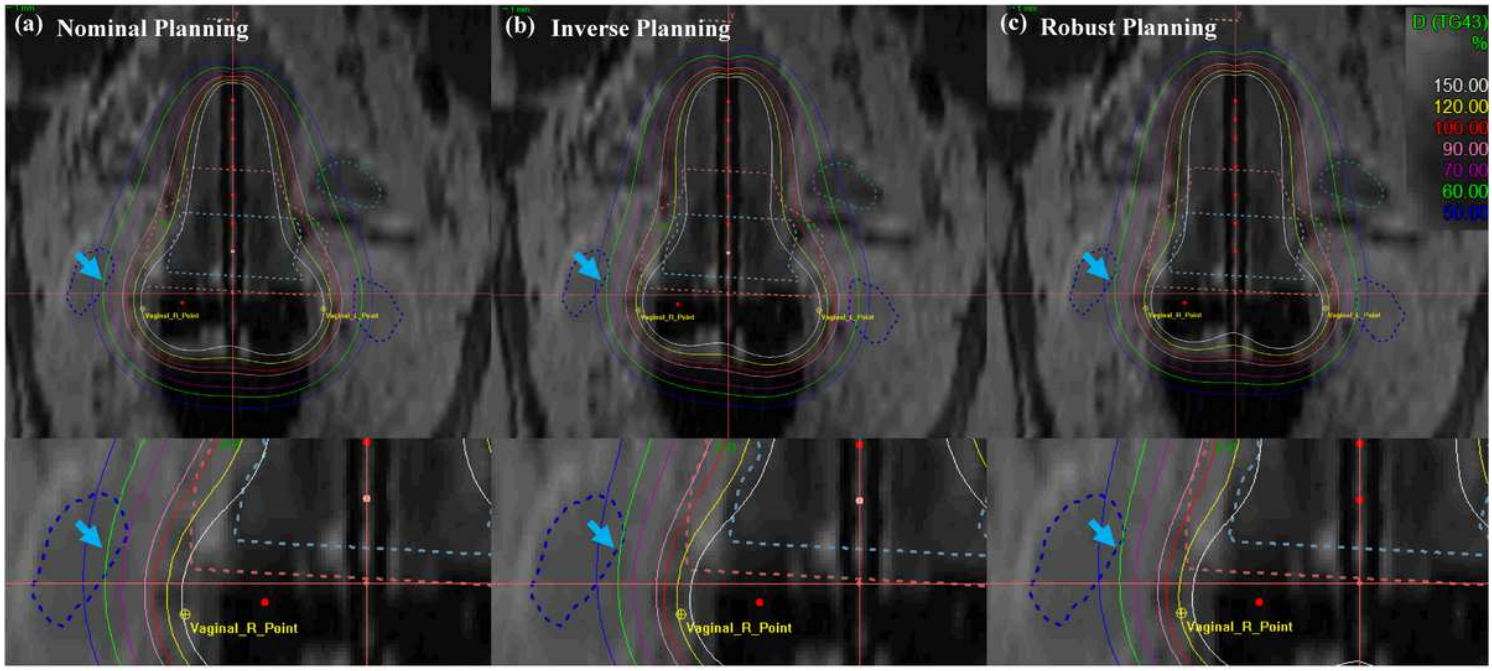

Figure 3

Iso-dose line comparison of (a) nominal (manual) planning, (b) inverse planning, and (c) robust planning standard planning in EBRT-BT boost treatment of cervical cancer: coronal view. An EBRT total dose of 5040 cGy was delivered in 28 fractions, and an ICR total dose of 3000 cGy was delivered in 6 fractions using a T&R applicator.

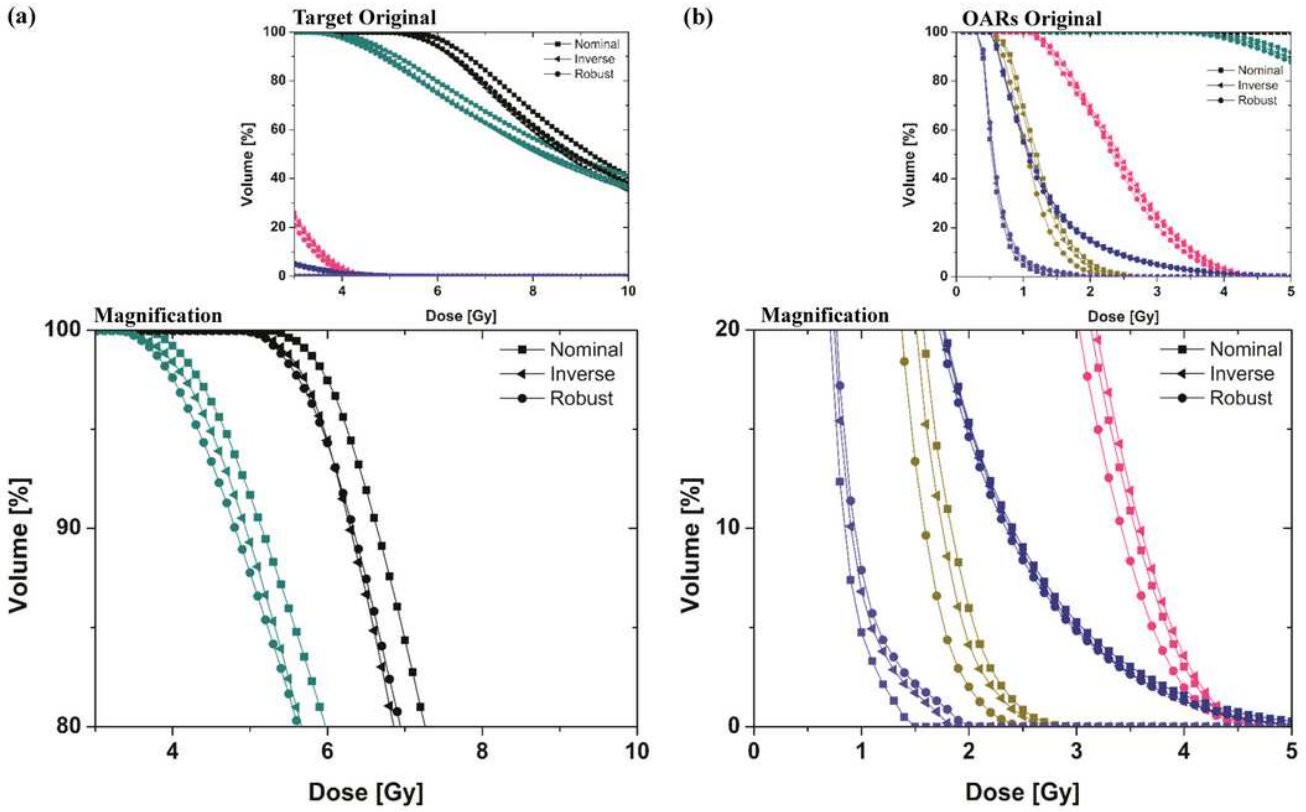

Figure 4

DVH curves for nominal (manual) planning, inverse planning, and robust planning in EBRT-BT boost treatment of cervical cancer were plotted using colors indicating: HRCTV-Black, IRCTV-Dark Cyan, Rectum-Dark Yellow, Sigmoid-Pink, Bladder-Royal, Bowel-Violet. Graphs (a) and (b) are the magnification of the DVH curves of the target and OAR.

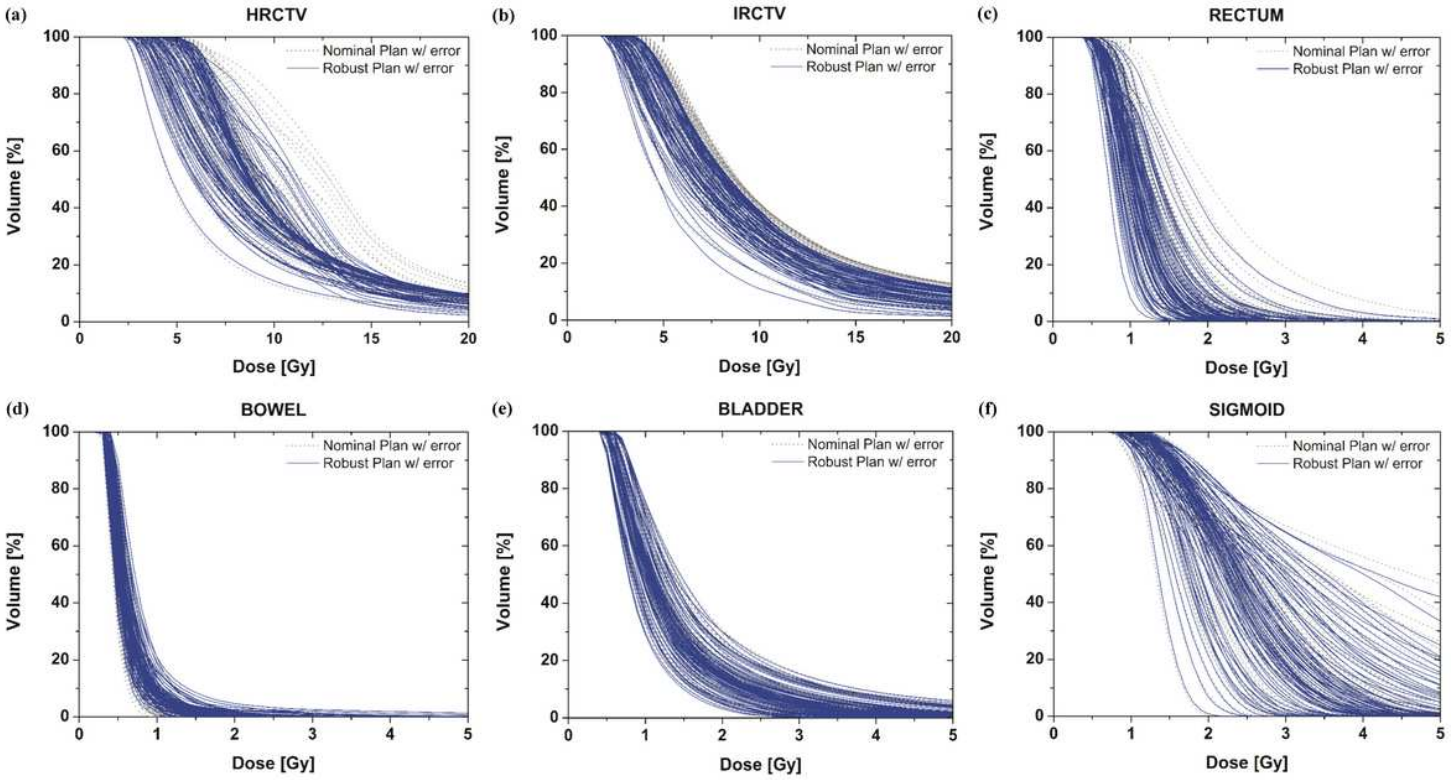

Figure 5

DVH curve variation of the targets (a)-(b) and OAR (c)-(f) under applicator positional errors with the shift scenario assumptions. DVHs from the robust, optimized plan with error scenarios are shown using a straight blue line, and the nominal DVHs of the non-robust plan with error scenarios are indicated by the grey dotted lines.

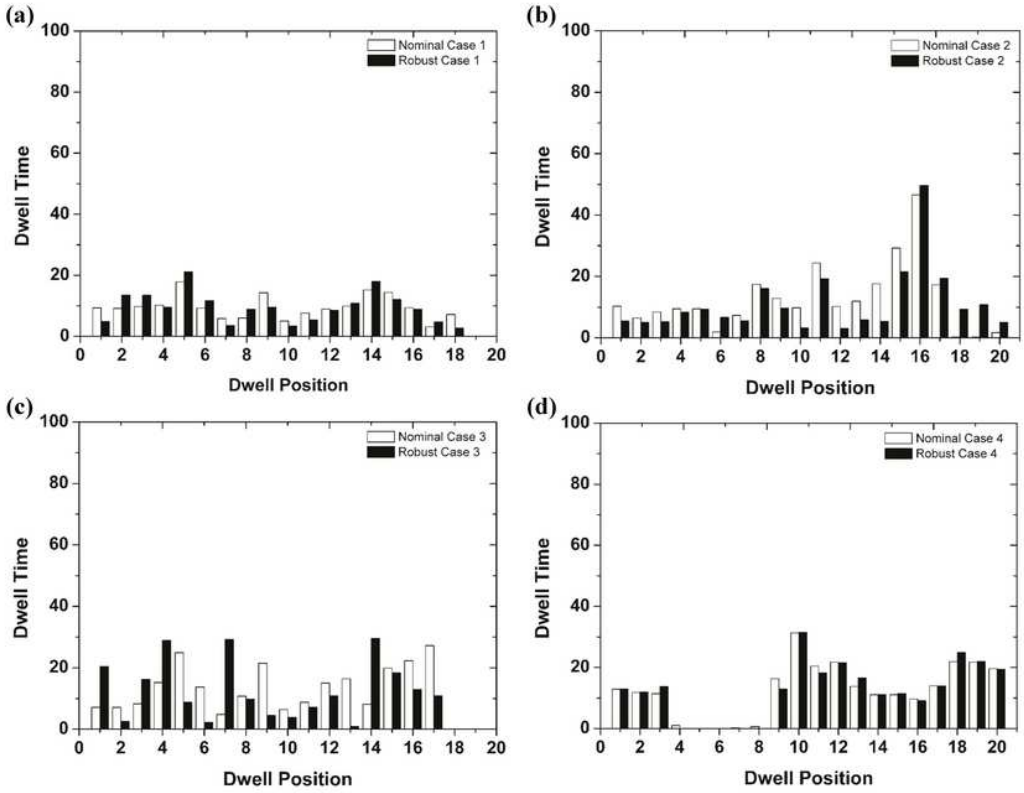

Figure 6

Distribution of dwell times along the tandem and ring applicators in four cases with robust planning. The corresponding dwell times for a manual optimization (nominal) is also presented for comparison: (a) case 1, (b) case 2, (c) case 3 and (d) case 4 are the each plan comparisons of distribution of dwell times.